RESEARCH ARTICLE | JULY 22 2026

Designing the ground state is not enough: Lessons from the self-assembly of Archimedean shells

Special Collection: Festschrift in honor of Christoph Dellago: Exploring Paths and Barriers in Statistical Mechanics

Luigi Graziano; Niccolò Tedeschi ; Petr Šulc ; John Russo ; Francesco Sciortino

J. Chem. Phys. 165, 044901 (2026)
https://doi.org/10.1063/5.0336907

The Journal of Chemical Physics ARTICLE pubs.aip.org/aip/jcp

Designing the ground state is not enough: Lessons from the self-assembly of Archimedean shells

Cite as: J. Chem. Phys. 165, 044901 (2026); doi: 10.1063/5.0336907
Submitted: 3 April 2026 • Accepted: 2 July 2026 •
Published Online: 22 July 2026

Luigi Graziano,[1] Niccolò Tedeschi,[2] Petr Šulc,[2,3] John Russo,[1] and Francesco Sciortino[1,a)]

AFFILIATIONS

[1] Dipartimento di Fisica, Sapienza Università di Roma, P.le Aldo Moro 5, 00185 Rome, Italy
[2] TU Munich, School of Natural Sciences, Department of Bioscience, Garching, Germany
[3] School of Molecular Sciences and Center for Molecular Design and Biomimetics, The Biodesign Institute, Arizona State University, 1001 South McAllister Avenue, Tempe, Arizona 85281, USA

Note: This paper is part of the Special Topic Festschrift in Honor of Christoph Dellago: Exploring Paths and Barriers in Statistical Mechanics.
[a)] **Author to whom correspondence should be addressed:** francesco.sciortino@uniroma1.it

ABSTRACT

Designing particle interactions such that a target structure is the thermodynamic ground state is a central paradigm in self-assembly. However, ensuring that the target is lowest in energy and that obvious competitors are energetically penalized does not, by itself, guarantee successful assembly at finite temperature, since even under these conditions competing structures can reappear as minima of the free-energy landscape. Focusing on the colloidal Archimedean snub-cube, we compute the full free-energy landscape of all competing aggregates using a cluster-based thermodynamic approach. While the target structure is uniquely selected at the level of potential energy, we find that competing clusters can become thermodynamically favored due to entropic contributions, particularly when bond directionality is high. In this regime, incomplete structures, such as icosahedra, are stabilized despite their higher energy per particle, leading to a dramatic suppression of the target yield. Our results provide quantitative guidelines for inverse design strategies that explicitly account for entropy, bond flexibility, and experimental conditions.

I. INTRODUCTION

Bottom-up self-assembly[1,2] refers to a design strategy in which the instructions required to build a pre-defined aggregate are encoded directly at the level of the individual particles.[3–8] Through an appropriate choice of particle shape, interaction anisotropy, and interaction strength, one aims to drive the spontaneous formation of a target structure, which may be finite[9–12] or infinite in extent (either ordered[13–16] or disordered[17]). This paradigm has proven extremely powerful and has been successfully applied to a wide range of systems, from molecular and colloidal assemblies to nanoparticle superlattices and metamaterials.

The implementation of bottom-up self-assembly has followed several complementary routes. In some cases, particles and interactions are rationally designed by human intuition and physical insight; in others, optimal designs are identified through extensive trial-and-error approaches or through inverse-design,[18–21] algorithmic optimization methods,[22–27] and machine learning approaches.[28–31] In parallel, significant progress has been achieved in the ability to engineer particle–particle interaction potentials with tailored functional forms,[30] as well as in the decoration of colloidal building blocks with highly selective, often binary, interactions.[32] These advances have greatly expanded the accessible design space and have enabled increasingly complex target structures to be specified at the outset.

Major advances have also been achieved in the experimental realization of addressable building blocks, particularly through DNA nanotechnology[33,34] and, more specifically, DNA-origami.[35,36]

In this approach, a long single-stranded DNA scaffold is folded into a prescribed three-dimensional shape using a large number of short complementary "staple" strands, enabling precise control over both particle geometry and the spatial arrangement of interaction sites. By functionalizing selected locations on the surface with specific DNA sequences, it is possible to encode highly selective, effectively binary interactions between particles, closely mimicking the patchy-particle models employed in theoretical studies. A wide variety of shapes, including cubes,[37] octahedra,[38] icosahedra,[16] and tetrapods,[39] have been realized experimentally, providing versatile platforms for programmable self-assembly.

In most of the inverse self-assembly approaches, the central guiding principle is to design particles such that the desired structure corresponds to the thermodynamic ground state of the system. The expectation is that, upon annealing or slow assembly, the system will naturally relax toward this minimum-energy configuration. However, despite highly optimized designs, the experimental or computational outcomes of self-assembly processes frequently fall short of these expectations. Kinetic constraints and out-of-equilibrium phenomena often interfere with the pathway toward the target structure, leading instead to dynamically arrested states, such as misassembled structures, glasses,[40] or gels.[41] Even more frustrating are situations in which the system does assemble into well-defined clusters or extended lattices, yet these structures differ from the intended target. In such cases, the assembly process is not merely arrested but is diverted toward competing local minima in the free-energy landscape, highlighting the critical role of kinetics, metastability, and assembly pathways in determining the final outcome.[42] These observations underscore the limitations of a design strategy based solely on ground-state stability and motivate the need for approaches that explicitly account for finite-temperature effects during self-assembly. Previous studies have already highlighted the need to move beyond a purely ground-state perspective in inverse design. Several approaches have explicitly incorporated finite-temperature effects and free-energy optimization into the design process, including relative-entropy optimization methods,[19] grand-canonical inverse-design strategies,[43] alchemical and landscape-engineering approaches,[20,22,27] and more recent machine-learning based inverse-design strategies.[29,30] These studies demonstrate that assembly behavior cannot, in general, be inferred solely from the energetic ground state, since entropy and finite-temperature effects can qualitatively modify the free-energy landscape.

One particularly illustrative case of this behavior is provided by the self-assembly of finite-size clusters,[44–46] for example, with Archimedean geometry.[47] The snub cube is a polyhedron with 38 faces (6 squares and 32 equilateral triangles), 60 edges, and 24 vertices, each connected to five neighbors. It can, thus, be assembled from 24 identical particles carrying five interaction sites. Each particle is the corner of one square and of three triangles, requiring a non-trivial location of the five contact points (the patches). As shown in Ref. 47, placing the five patches according to the geometry of the corresponding contact points leads, *in silico*, to successful assembly of the snub cube under appropriate temperature and density conditions.

To move toward experiments, it is necessary to synthesize bulk quantities of patchy particles. A natural experimental realization of such building blocks is offered by DNA-origami based particles, where interaction patches can be positioned with high spatial precision. In particular, an icosahedral DNA-origami structure provides a convenient scaffold: selecting five vertices connected to a given vertex defines a five-patch particle with fixed geometry. These five sites can be functionalized with specific DNA sequences to encode selective interactions between particles, effectively implementing an addressable interaction scheme. We stress that to find a DNA-origami with exactly the required geometries to satisfy the optimal contact to self-assemble the snub-cube, while in principle not impossible, is quite difficult. To ease the experimental realization of the numerical findings, it is then easier to select a particle shape whose vertices are, with a small angular variation, compatible with the required geometry. This is achieved by adding a short DNA strand preceding the sticky sequence, to increase the binding angular range. Luckily, the five vertices of the icosahedron (the green ring in Fig. 1) are very close to the optimal patch positions requested to assemble the snub-cube and, with a minimal angular opening, patchy particles with the icosahedron geometry can generate a fully bonded snub-cube.

In this work, we use this experimentally realizable system as a prototypical example to investigate the limits of ground-state-based design strategies and to assess the role of the mismatch in the patch locations. While interactions can be engineered such that the snub cube is the unique ground-state structure, this does not guarantee its formation under realistic conditions. In particular, the geometric mismatch between the ideal target structure and the actual arrangement of patches on the building blocks, together with the finite angular flexibility of the bonds, introduces additional degrees of freedom that affect the thermodynamics of assembly. In particular, we investigate here the influence of the opening of the patch angle on the yield of the snub-cube across a wide range of temperatures and particle concentrations. We do so exploiting the ideal-gas-of-clusters thermodynamic formalism.[48] This theoretical framework, which assumes that particle concentrations are sufficiently low (a condition often satisfied in DNA-origami based experiments), allows for the calculation of the probability of observing any possible aggregate in the system. In essence, it provides a quantitative map of which cluster configurations are thermodynamically favored under given experimental conditions. The formalism requires as input the partition function of all thermodynamically relevant clusters, a quantity that can be computed numerically using established methodologies (see Method section). In this work, we evaluate these partition functions for three distinct values of bond flexibility, providing insight into how the mechanical properties of the patches influence self-assembly. Our calculations reveal that, in all cases, the snub-cube represents the ground-state structure. However, only when the bonding angle is sufficiently large can the yield of the snub-cube approach unity for realistic experimental particle concentrations and accessible temperature ranges. We further show that increasing bond flexibility enhances the number of microstates in which a patch–patch bond can form, effectively increasing the bonding entropy. This entropic contribution has a substantial impact on the free energy of clusters and can even override energetic considerations in certain regimes. In particular, at temperatures where bonds are not irreversibly formed, clusters with higher bonding energies, corresponding to finite size structures with unformed bonds, can

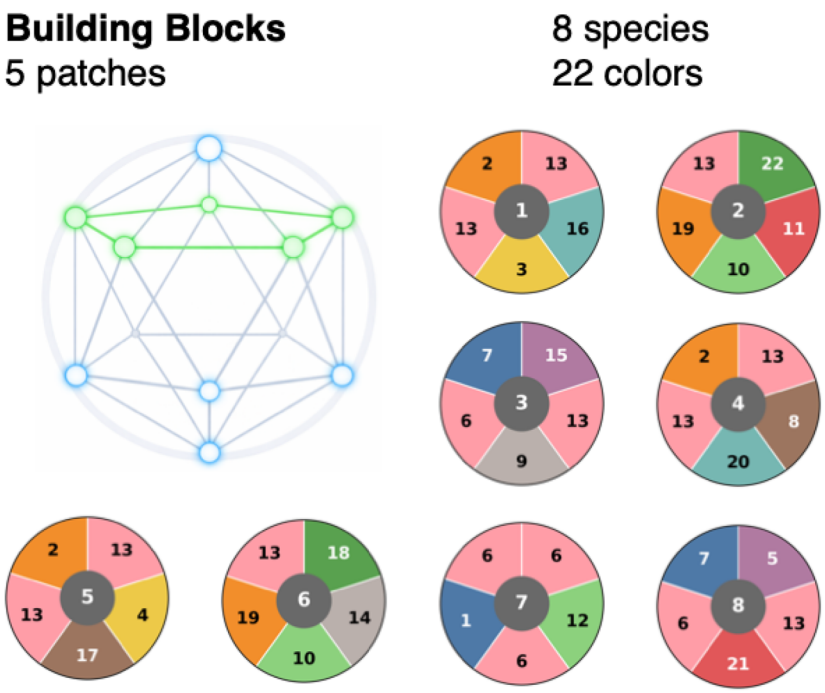

FIG. 1. Cartoon of the building blocks. Each particle is modeled as a sphere decorated with five interaction patches positioned at selected vertices (green) of an inscribed icosahedron. The eight species are shown as disks, where the five sectors represent the patch positions and the numbers indicate the assigned interaction colors. Patches with different number but sharing the same color are complementary and form specific bonds.

become thermodynamically preferred over the snub-cube. As a consequence, the yield of the snub-cube can be drastically reduced under these conditions.

Overall, our results highlight the predictive power of the gas-of-clusters formalism and demonstrate the effectiveness of the methodology for calculating cluster free energies. They provide a clear strategy for optimizing experimental parameters, such as bond flexibility, particle concentration, and temperature, to maximize the formation of the desired snub-cube structure.

II. METHODS

A. Coloring problem

We explore the self-assembly of finite-size clusters formed by a mixture of eight distinct patchy particles. Each particle is modeled as a sphere decorated with five interaction sites (patches), positioned on five adjacent vertices of a dodecahedron inscribed in the sphere (Fig. 1). This choice of geometry is experimentally motivated: recent advances in DNA nanotechnology have enabled the realization of highly programmable building blocks based on wireframe DNA-origami, including icosahedral particles with addressable vertices that can be selectively functionalized with binding sites.[16] In these systems, patches correspond to specific DNA sequences placed at prescribed locations on the DNA-origami scaffold, providing a direct route to implementing patchy-particle designs.

The system consists of eight particle species carrying a total of 40 interaction patches. The number of species is the minimum number that satisfies all the bonding constraints imposed by the SAT-assembly design discussed in Appendix B. Each patch is assigned an interaction type determined through the SAT-assembly procedure.[23,49] The full specification of the building blocks is summarized graphically in Fig. 1, where each species is represented together with the corresponding patch interactions.

Interactions between patches are pairwise: each patch type is complementary to exactly one other patch type. In Fig. 1, interacting patches are represented with the same color. The explicit assignment of patch colors to each species, together with the list of complementary color pairs obtained from the SAT construction, is reported in Appendix B.

The SAT-assembly solution guarantees that the 24-particle snub-cube (formed by 2, 3, 3, 2, 2, 3, 6, and 3 particles for each species; see Fig. 2) is the unique fully bonded ground-state cluster, at least for cluster sizes up to 30. Alternative aggregates can, in principle, form, but they are necessarily characterized by the presence of unsatisfied patches and, therefore, lie at higher energy.

A relevant competing structure is the 12-particle icosahedron. While this geometry can be assembled, the SAT solution enforces frustration in the bonding pattern: not all nearest-neighbor contacts can be satisfied simultaneously. In fact, the SAT construction[23] guarantees that any icosahedral assembly must contain at least five unsatisfied bonds. One of the many possible 12 particle configurations encountered in simulations is shown in Fig. 2. In this specific 12-particle cluster, seven bonds are broken (highlighted in red), resulting in only 23 satisfied bonds out of the 30 possible in a fully bonded icosahedron. For comparison, Fig. 2 shows the fully bonded snub-cube cluster (60 out of 60 bonds).

B. Simulation methods

The particles interact with the Kern–Frenkel model,[50,51] a model describing the colloidal particle as a hard sphere of diameter σ decorated by a finite number of patches with angular width θ on its surface. The particle–particle interaction potential $U(\mathbf{r}_{ij}, \Omega_i, \Omega_j)$

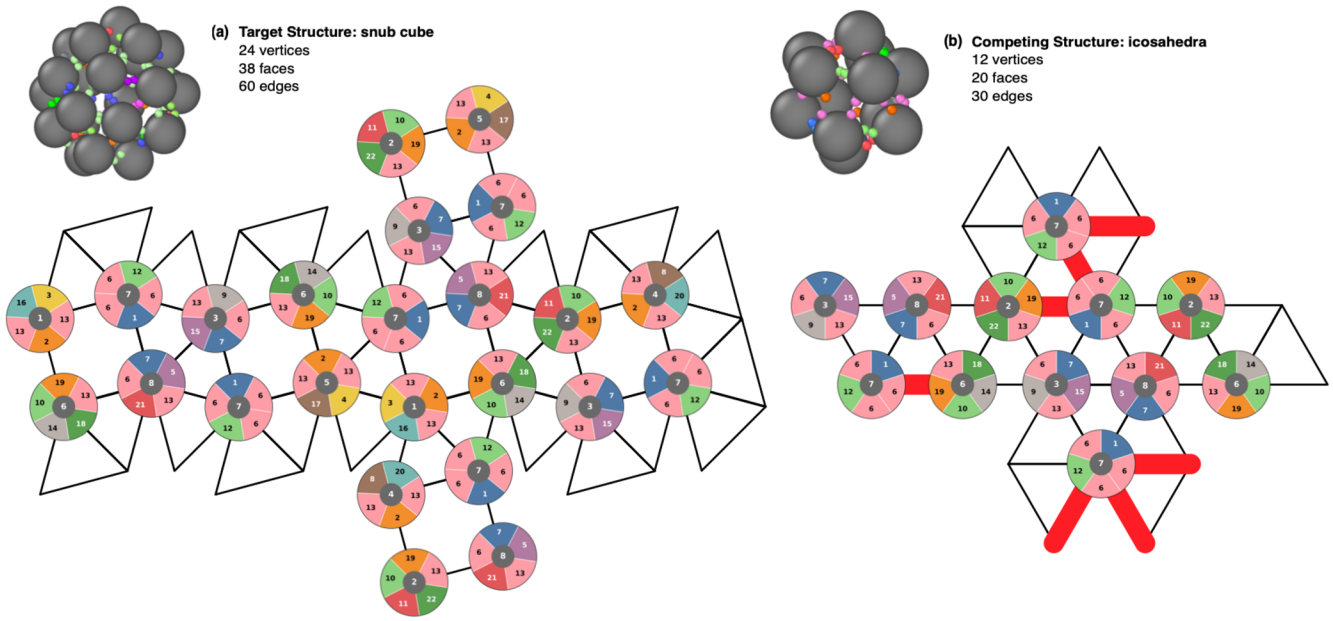

FIG. 2. Target and competing assemblies. (a) The designed ground-state structure, a snub cube composed of 24 particles, shown together with its planar net representation and the corresponding assignment of particle species. (b) One of the many possible competing icosahedral structure formed by 12 particles. The same interaction scheme is projected onto the icosahedron; however, due to geometric incompatibility, not all designed bonds can be satisfied. In this representation, seven bonds are broken, highlighted by red lines.

TABLE I. Cartesian coordinates of the five patches on a sphere of diameter $\sigma = 1$ implemented in the numerical calculations. On the plane on which all five patches are sitting, the angle between consecutive patches is 72°. In the snub-cube case, always on the plane containing the patches, the five angles are, respectively, 99.3°, 65.2°, 65.2°, 65.2°, 65.2°. Calculated from the origin, the five angles between consecutive patches of the icosahedra are 60°, while they are 90°, 60°, 60°, 60°, 60° for the snub cube.

Patch No.	x	y	z
1	−0.425 325 5	0.000 000 0	−0.212 662 5
2	−0.131 433 0	0.404 508 5	−0.212 662 5
3	0.344 095 5	0.250 000 0	−0.212 662 5
4	0.344 095 5	−0.250 000 0	−0.212 662 5
5	−0.131 433 0	−0.404 508 5	−0.212 662 5

between particles i and j with center of mass distance $\mathbf{r}_{ij}$ and orientation Ω_i and Ω_j is described by a square well of width Δ and depth ϵ as

$$U(\mathbf{r}_{ij}, \Omega_i, \Omega_j) = \begin{cases} +\infty, & r_{ij} < \sigma, \\ -\varepsilon\, f(\hat{\mathbf{r}}_{ij}, \Omega_i, \Omega_j), & \sigma \le r_{ij} \le \sigma + \Delta, \\ 0, & r_{ij} > \sigma + \Delta, \end{cases} \quad (1)$$

where $\hat{\mathbf{n}}_{i\alpha}$ denotes the location of the patch α on particle i and $\hat{\mathbf{n}}_{j\beta}$ denotes the location of the patch β on particle j,

$$f(\hat{\mathbf{r}}_{ij}, \Omega_i, \Omega_j) = \begin{cases} 1, & \hat{\mathbf{r}}_{ij} \cdot \hat{\mathbf{n}}_{i\alpha} \ge \cos\theta \text{ and } -\hat{\mathbf{r}}_{ij} \cdot \hat{\mathbf{n}}_{j\beta} \ge \cos\theta, \\ 0, & \text{otherwise.} \end{cases} \quad (2)$$

The coordinates of the five patches, located on the surface of a sphere of diameter $\sigma = 1$, are reported in Table I.

In the following, we choose ϵ as unit of energy and σ as unit of length. Selecting $k_B = 1$, the temperature is in unit of ϵ. In the numerical simulations, we have explored three values of the opening patch angle $(\cos\theta = 0.93, 0.96, 0.98)$, keeping fixed the interaction range to $\Delta = 0.2\sigma$. We have explored a range of temperatures $(k_B T/\epsilon = 0.18, 0.16, 0.14, 0.12, 0.10)$ where it was possible to equilibrate the system during the simulation.

C. Numerical evaluation of the cluster free energy

To calculate the free energy of all possible finite size clusters, we extend the formalism first proposed in Ref. 52 for one-component systems, and later on applied to study clustering in patchy colloids[53] and in dipolar hard spheres[54] to the present multicomponent system. With this formalism, it becomes possible to calculate the free energy of each cluster type and, as a consequence, to predict the yield of each aggregate as a function of the sample density and temperature. We use here an equilibrium definition of yield, assuming that the self-assembly process can proceed to thermodynamic equilibrium. In experiments, often kinetic traps significantly alter the expected yield. The idea of the method is to perform a *cluster* grand canonical Monte Carlo (CGCMC) simulation, i.e., a grand canonical simulation at fixed chemical potential μ_k of each specie k, with the constraint that the N particles in the simulated volume V form a single cluster. For the multi component system composed by s particle types that we study, the corresponding s values of the activities $(z_k \equiv e^{\beta\mu_k})$ are chosen proportional to the composition of

the target structure, which coincides also with the composition of the experimental sample and are in the following grouped in the symbol $\{z\}$.

A cluster of size N is defined as a set of N particles connected via a continuous path of bonds. Two particles are defined as bonded if their pair interaction energy is $-\epsilon$, i.e., if a patch–patch interaction is present between them. The CGCMC algorithm, described in more details in Appendix A, evolves the cluster by adding particles bonded to existing ones or eliminating particles, which do not break the cluster in two (or more) pieces. Clusters are labeled according to their composition and energy. In the following, we indicate with $\{m\}_\alpha$ the set of numbers providing the cluster composition (the number n_i of particles of species i in the cluster α) and with E the cluster energy. The index α runs from 1 to the number of different clusters observed in the simulation. $\alpha = 1$ is, by definition, the cluster composed by one monomer of type 1, with energy 0. An histogram of the relative occurrence of each cluster provides a measure of the cluster partition function. We note on passing that the sampled clusters will differ in their composition.

To parallelize the calculation and to force the simulation to explore the entire range of N values, from 1 to $N_{\max}$ (a value of $N_{\max} \approx 35$–40 allows to sample all relevant clusters), we have encoded a successive umbrella sampling,[55] by separating the range $1 - N_{\max}$ into several overlapping sub-ranges covering the entire N interval. While the choice of $N_{\max}$ may appear arbitrary, its validity can be a posterior checked by looking at the behavior of the resulting cluster size distribution close to $N_{\max}$ for any reasonable value of the sample number density. In each window, the amplitude of the z_i values (proportional to the target composition) is optimized by trial and error to provide an accurate sampling of the entire window.

After merging the results from different windows (reweighting the results to a chosen set of z_i values), we calculate the probability $P(\{m\}_\alpha, \{z\}, T)$ of observing the cluster α at temperature T when the activities are $z_1, z_2, \ldots, z_s$. The probability is proportional to the cluster partition function $Z(\{m\}_\alpha, T)$ as

$$P(\{m\}_\alpha, \{z\}, T) = \frac{z_1^{n_1} z_2^{n_2} \ldots z_s^{n_s} Z(\{m\}_\alpha, T)}{\Omega}, \tag{3}$$

where Ω is the normalization. Dividing both sides by $P(\{m\}_1, \{z\}, T)$, and inverting this relation, one obtains the cluster partition functions (in the canonical ensemble, i.e., quantities which do not depend on the activity values chosen in the CGCMC),

$$\frac{Z(\{m\}_\alpha, T)}{Z(\{m\}_1, T)} = \frac{1}{z_1^{n_1 - 1} z_2^{n_2} \ldots z_s^{n_s}} \frac{P(\{m\}_\alpha \{z\}, T)}{P(\{m\}_1, \{z\}, T)}. \tag{4}$$

Note that since $Z(\{m\}_1, T)$ is simply a measure of the volume available to a monomer, the ratio $\frac{Z(\{m\}_\alpha, T)}{Z(\{m\}_1, T)}$ is de facto the partition function of the cluster at fixed center of mass. Thus, $F_\alpha(T)$, the free energy of the cluster α, the quantity that concurs to control the probability of observing that specific cluster, i.e., the yield of that cluster, is exactly given by

$$F_\alpha(T) = -k_B T \ln \frac{Z(\{m\}_\alpha, T)}{Z(\{m\}_1, T)}. \tag{5}$$

In addition, since the cluster energy is known, it is possible to estimate the cluster entropy as

$$\frac{S_\alpha(T)}{k_B} = \beta E_\alpha - \beta F_\alpha(T). \tag{6}$$

Once the partition functions are known, it becomes possible to predict the cluster composition of dilute systems at any temperature. Indeed, in the ideal gas of cluster approximation, in which the cluster-cluster interactions are neglected, the probability of observing any cluster type, knowing the average composition of the system, can be calculated.[48,56]

To start with, we define ρ_i as the number density of species i (total number of particles of species i in the volume V). Note that in experiments, in preparing the sample, one controls the s values of ρ_i and their sum $\rho = \sum_{i=1}^{s} \rho_i$, the total number density (total number of particles in the volume V). Other quantities are dependent on the outcome of the aggregation process, and as such, they depend on temperature: $\rho_{i,1}$ is the monomer number density for species i (total number of particles of species i in monomeric form in the volume V) and ρ_N is the number density of clusters of size N (total number of clusters of size N in the volume V, the cluster size distribution). The $\rho_{i,1}$ values provide the activities of the s species. Indeed, assuming thermodynamic equilibrium, particles can exchange between different clusters, indicating that the chemical potential of a particle type is identical in all clusters containing that particle.[48,56] Hence, the chemical potential coincides with the one of the particle in monomeric state. Being an ideal gas of non-interacting clusters, this chemical potential is known, and the corresponding activity coincides with the monomer density.[48] In the ideal gas of cluster, the probability to observe the cluster α is

$$P(\{m\}_\alpha, T) = \rho_{1,1}^{n_1} \rho_{2,1}^{n_2} \ldots . \rho_{s,1}^{n_s} \frac{Z(\{m\}_\alpha, T)}{Z(\{m\}_1, T)}. \tag{7}$$

Since the values of $\rho_{i,1}$ are not *a priori* known, to calculate them from the known ρ_i values, we implement an iterative procedure. We start from arbitrary initial values $\rho_{i,1}$ and predict ρ_k as

$$\rho_k = \sum_\alpha \rho_{1,1}^{n_1} \rho_{2,1}^{n_2} \ldots . \rho_{s,1}^{n_s} \frac{Z(\{m\}_\alpha, T)}{Z(\{m\}_1, T)} n_k. \tag{8}$$

Then, if the calculated ρ_k differ from the desired values, the monomer densities $\rho_{k,1}$ are correspondingly changed and the process is iterated until convergence is reached for all species.

Once the desired values of $\rho_{k,1}$ are found for all k, one can calculate the number density of clusters of size N,

$$\rho_N(T) = \sum_\alpha \rho_{1,1}^{n_1} \rho_{2,1}^{n_2} \ldots . \rho_{s,1}^{n_s} \frac{Z(\{m\}_\alpha, T)}{Z(\{m\}_1, T)} \delta\left(\sum_{i=1}^{s} n_i - N\right). \tag{9}$$

Summing over all partition functions with the same N, it is possible to evaluate the free energy for clusters of size N (independent from their shape) as

$$\beta F(N, T) = -\ln\left[\sum_\alpha \frac{Z(\{m\}_\alpha, T)}{Z(\{m\}_1, T)} \delta\left(\sum_{i=1}^{s} n_i - N\right)\right], \tag{10}$$

$$= -\ln\left[\sum_{\alpha} e^{-\beta F_{\alpha}(T)}\delta\left(\sum_{i=1}^{s} n_i - N\right)\right], \tag{11}$$

and the energy averaged over all clusters α with the same $N = \sum_{i=1}^{s} n_i$ by weighting the energy of each cluster with its partition function,

$$E(N) = \frac{\sum_{\alpha} E_{\alpha} e^{-\beta F_{\alpha}} \delta(\sum_{i=1}^{s} n_i - N)}{\sum_{\alpha} e^{-\beta F_{\alpha}} \delta(\sum_{i=1}^{s} n_i - N)}. \tag{12}$$

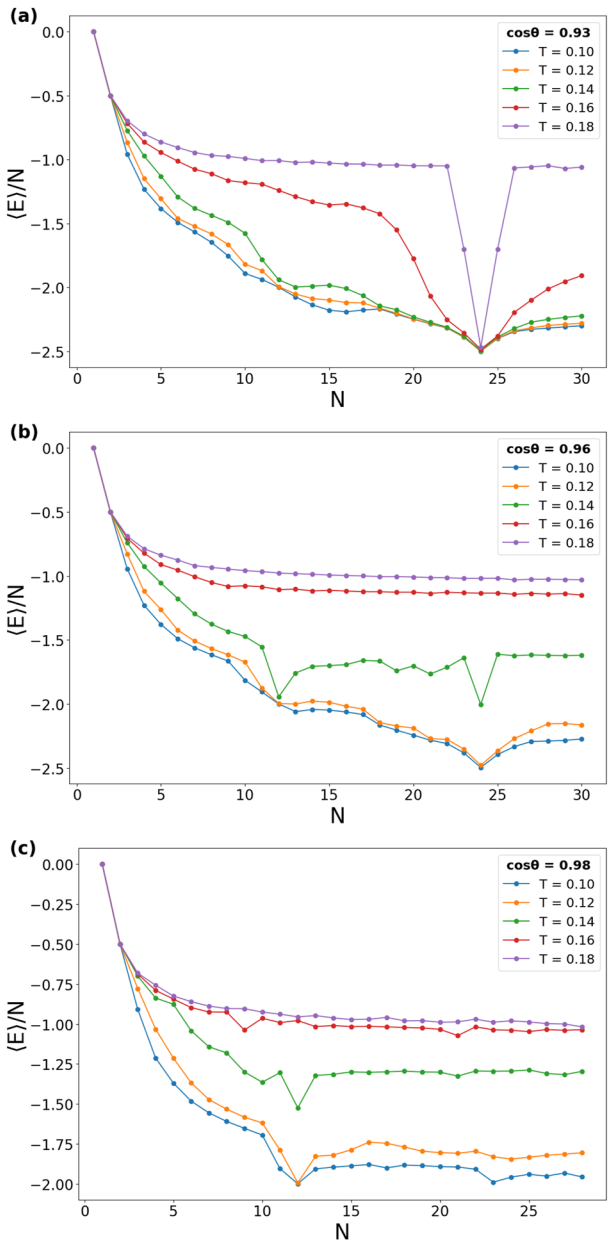

FIG. 3. Average potential energy per particle as function of cluster size N reported in units of ϵ for the five temperatures explored by the CGCMC simulations for three values of the patch angle [$\cos\theta = 0.93$ (a), $\cos\theta = 0.96$ (b) and $\cos\theta = 0.98$ (c)].

III. RESULTS

A. Energy vs free energy

Figure (3) shows $E(N)$ for the three different patch angles and for all explored temperatures. As imposed by the SAT-assembly design, the lowest possible energy per particle ($E/N = -2.5$), corresponding to all patch–patch interactions satisfied, is observed

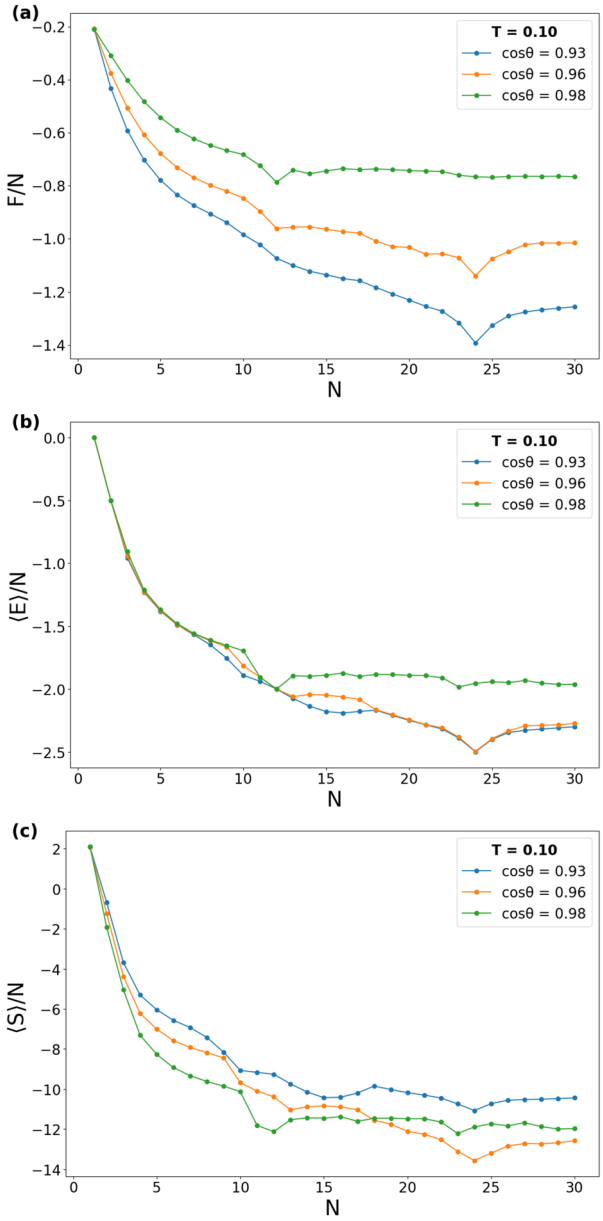

FIG. 4. (a) Comparison between free energy per particle as function of cluster size N for the three explored angles at $T = 0.10$. Local minima of $F(N)$ are observed at $N = 12$ for $\cos\theta = 0.98$ and at $N = 24$ for $\cos\theta = 0.93$. (b) Comparison between average potential energy per particle as function of cluster size N for the three explored angles at $T = 0.10$. (c) Comparison between average entropy per subunit as function of cluster size N for the three explored angles for $T = 0.10$.

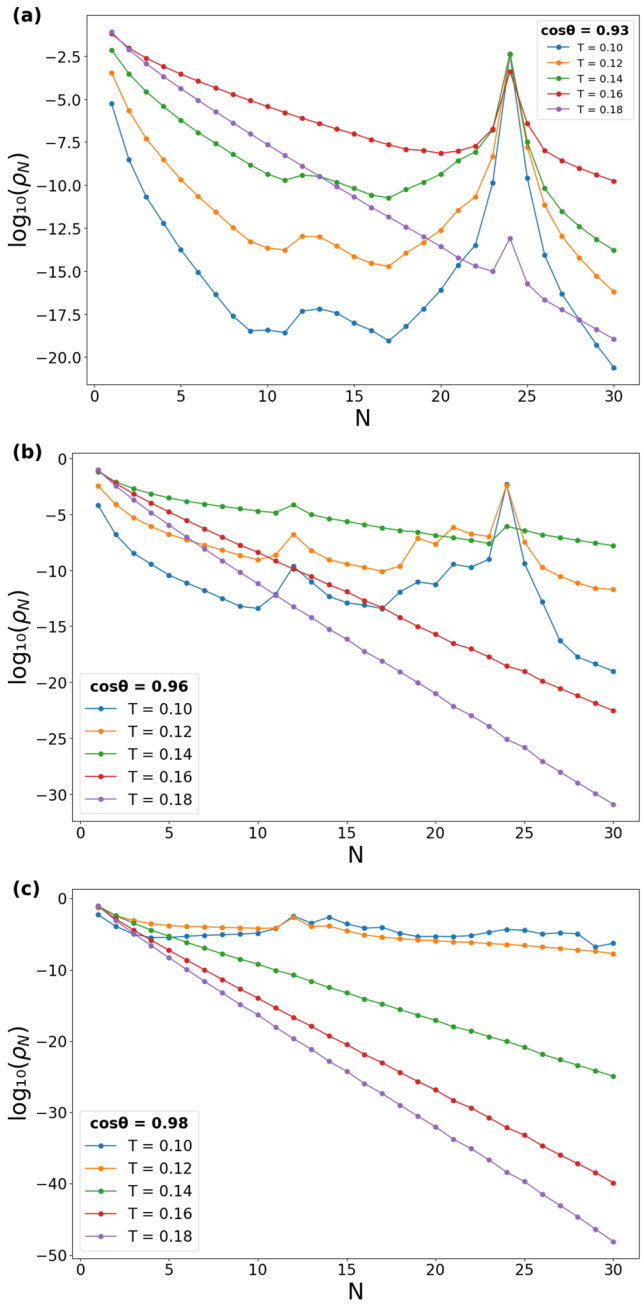

FIG. 5. Number density ρ_N of clusters in semi-log scale as function of size N for the explored range of temperatures in the three sampled patch geometries: panel (a) $\cos\theta = 0.93$, panel (b) $\cos\theta = 0.96$, and panel (c) $\cos\theta = 0.98$. The total number density is $\rho = \sum_{i=1}^{s} \rho_i = 0.1$. In any situation, the assembly mixture respects the stoichiometric ratios predicted for the target snub-cube.

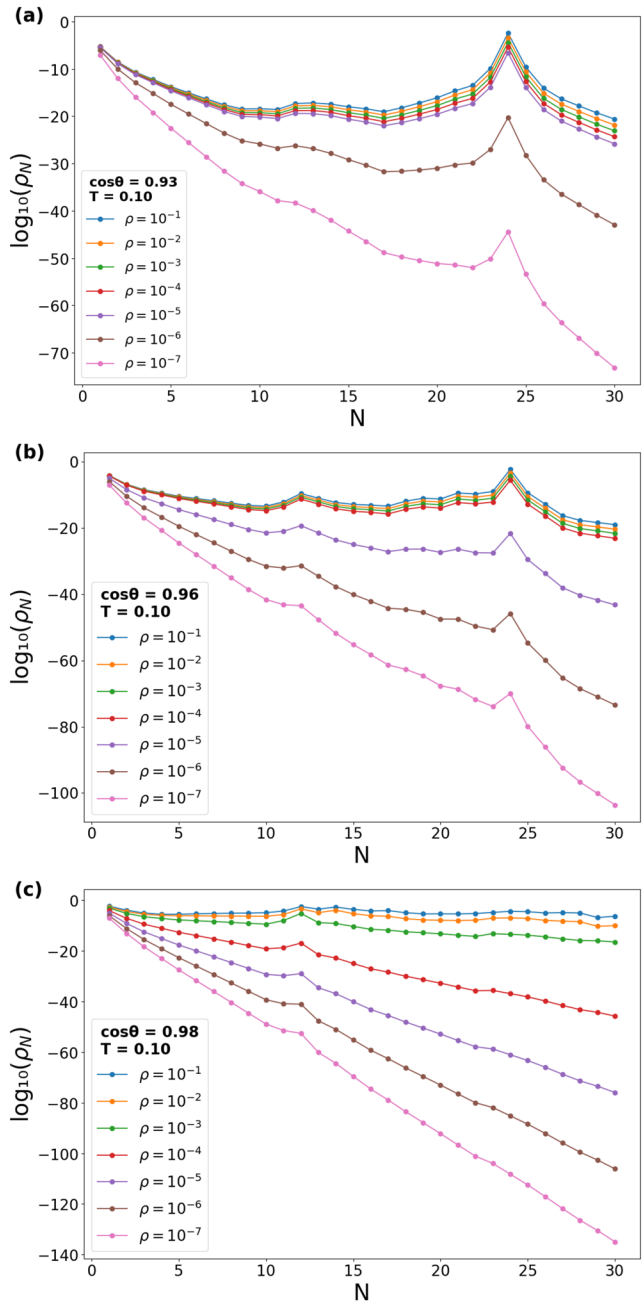

FIG. 6. Number density ρ_N of clusters in semi-log scale as function of size N for $T = 0.10$ and for $\rho = \sum_{i=1}^{s} \rho_i = 10^{-1}, 10^{-2}, 10^{-3}, 10^{-4}, 10^{-5}, 10^{-6}, 10^{-7}$. Panel (a) refers to $\cos\theta = 0.93$, panel (b) to $\cos\theta = 0.96$, and panel (c) to $\cos\theta = 0.98$.

only for the target snub-cube, but only for the two largest angles ($\cos\theta = 0.93$ and $\cos\theta = 0.96$). In the explored T region, the ground state (despite being geometrically possible) is never reached for any cluster size when $\cos\theta = 0.98$, suggesting that when the bonds are very directional, a small mismatch between the optimal geometry and the actual geometry encoded in the DNA-origami building block may prevent the formation of the target structure.

For the two largest patch angles ($\cos\theta = 0.93$ and $\cos\theta = 0.96$), the lowest explored temperatures are sufficient to reach the ground state. In this regime, the energy landscape is dominated by the target

structure, and the snub-cube at $N = 24$ emerges as the only pronounced minimum of $E(N)$, corresponding to the fully bonded configuration. All other cluster sizes lie at higher energy, indicating that the energetic design successfully suppresses competing structures at the level of potential energy.

To assess the role of entropy, in Fig. 4, we compare the free energy $F(N)$, average potential energy $E(N)$, and entropy $S(N)$ at the lowest investigated temperature ($T = 0.10$). The free-energy landscape reveals a qualitatively different scenario. While the energy landscape favors exclusively the snub-cube, the free energy reflects a competition between energy and entropy. For $\cos\theta = 0.98$, the only minimum of $F(N)$ occurs at $N = 12$, corresponding to the icosahedral cluster. For the intermediate angle $\cos\theta = 0.96$, both the icosahedron ($N = 12$) and the snub-cube ($N = 24$) appear as local minima, indicating coexistence between competing assembly pathways. Finally, for the widest angle $\cos\theta = 0.93$, the snub-cube becomes the only stable free-energy minimum.

These results demonstrate that, despite being energetically penalized due to unsatisfied bonds, the icosahedral cluster can be stabilized by entropic contributions and can dominate the assembly at finite temperature.

B. Cluster size distributions

To infer the probability of different clusters, we calculate the cluster size distribution for the three angles, at different temperatures, assuming the snub-cube composition as the sample composition. The total density, in Fig. 5, is fixed to $\rho = \sum_{i=1}^{s} \rho_i = 0.1$, but similar plot can be calculated for any desired sample density ρ. We show the cluster size distribution as number density of clusters ρ_N, i.e., with the normalization

$$\sum_N N\rho_N = \rho. \tag{13}$$

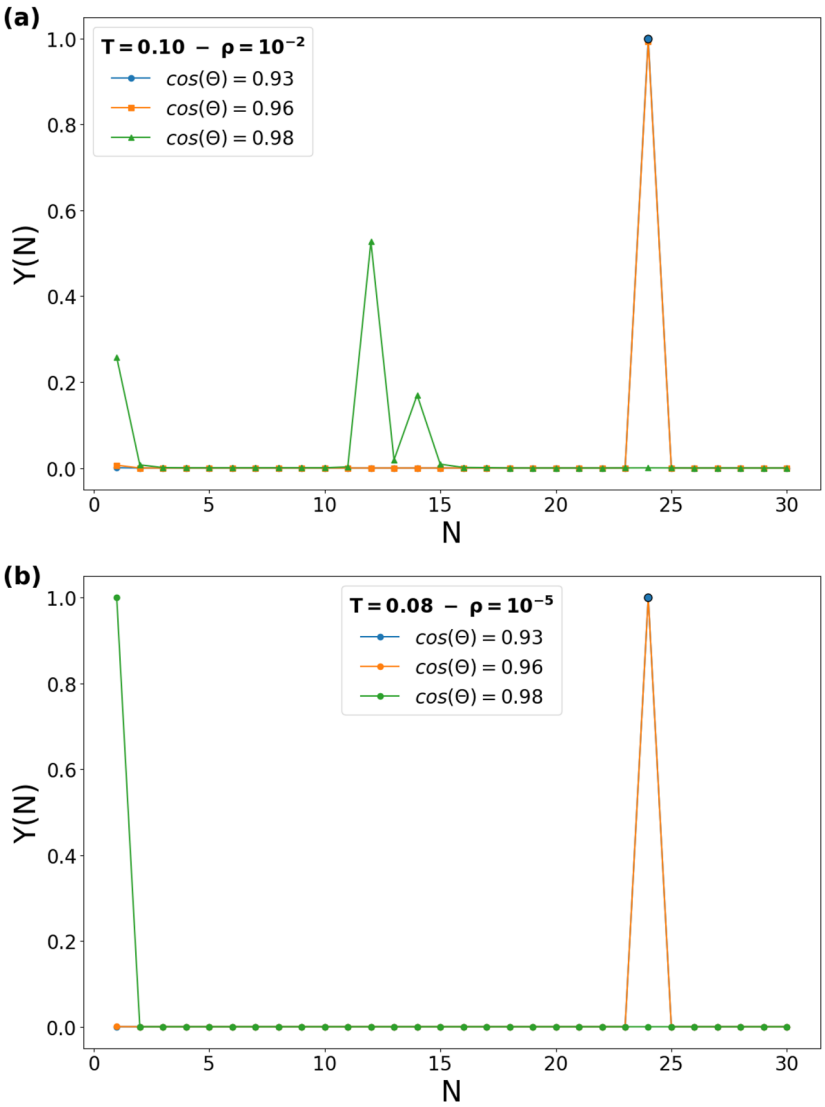

FIG. 7. Yield as function of cluster size N for the 3 different sampled patch geometries and for total density $\rho = 0.01$ and $T = 0.10$ in panel (a) and for $\rho = 10^{-5}$ and $T = 0.08$ in panel (b). Note that the results for $\cos\theta = 0.93$ and $\cos\theta = 0.96$ are very similar (almost superimposed and hard to discriminate).

Figure (5) shows that when $\rho = 0.1$, the cluster number density ρ_N evolves on cooling from a monotonically decaying distribution (almost exponential) to a structured function, with defined peaks. At low temperature, the dominant peak is found for the snub-cube ($N = 24$) for large angles and for the icosahedron ($N = 12$) for $\cos\theta = 0.98$.

Experiments based on DNA-origami particles are commonly run with much smaller densities ($\rho \approx 10^{-7}$–10^{-6}) and at the end of a slow scan in temperature, to favor the establishment of equilibrium. It is, thus, important to investigate the density evolution of the cluster size distribution. Figure 6 shows the behaviors of $\rho(N)$ for seven logarithmically spaced values of ρ at $T = 0.10$, the coldest temperature we have investigated numerically. The expected common trend is observed. From a system composed essentially of monomers at low density (note the logarithmic scale), on increasing density, the system evolves toward a coexistence of monomers and snub-cubes and then to mostly only snub-cubes but only for large patch angles. For the most directional angle ($\cos\theta = 0.98$), the incompletely bonded dodecahedra becomes the dominant aggregate.

C. Yield

An alternative picture of the same data is provided by the density dependence of the yield. The yield of clusters of size N, defined as the fraction of particles composing clusters of size N, is

$$Y(N) = \frac{N\rho_N}{\rho}, \quad \text{such that} \quad \sum_N Y(N) = 1. \tag{14}$$

Figure 7 shows the yield $Y(N)$ for the three patch angles at $T = 0.10$ with density $\rho = 0.01$ and at temperature $T = 0.08$ for a density comparable to a typical experimental one $\rho = 10^{-5}$.

At the temperature where the ground state structures are sampled, the cluster size distribution becomes essentially a δ function centered on the snub-cube for the two large angle solutions,

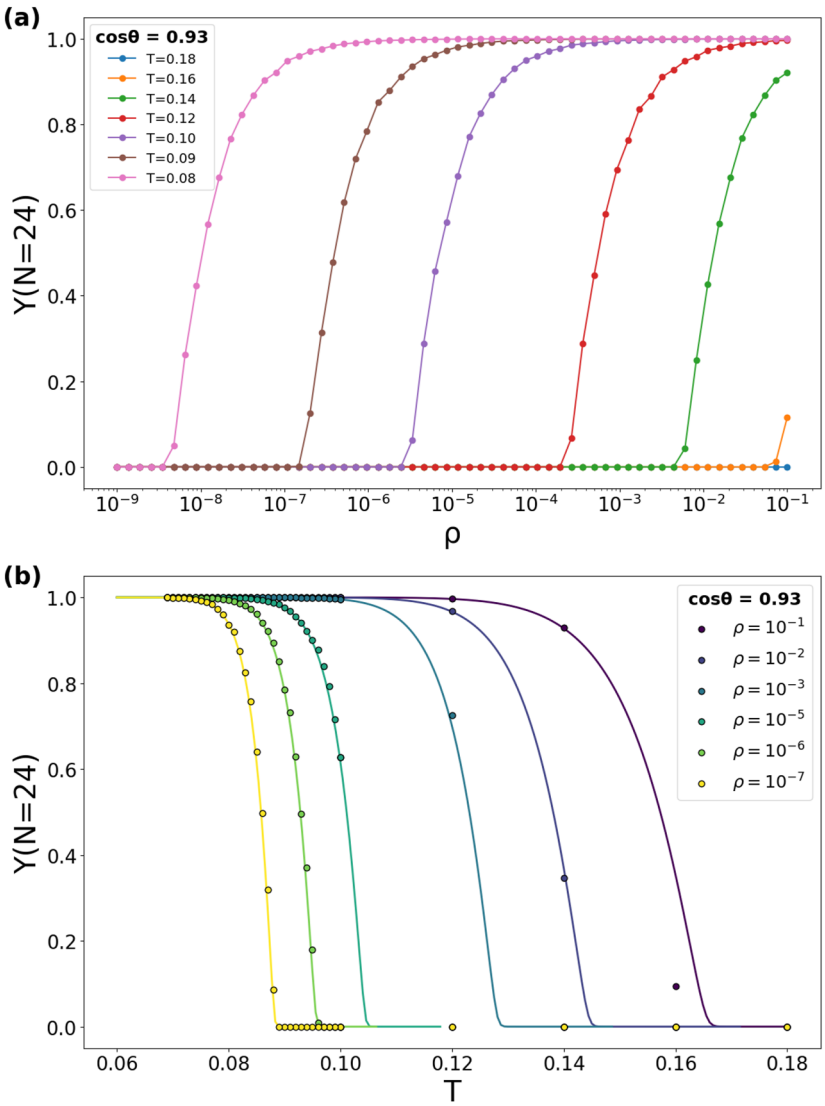

FIG. 8. Yield of $N = 24$ aggregate for patch geometry $\cos\theta = 0.93$ (a) as a function of total density ρ and (b) as a function of T.

confirming the SAT design prediction.[47] As shown in Appendixes C and D, in this condition, a theoretical description based only on monomers and snub-cubes provides an excellent description of the yield. For the more directional case, the snub-cube never appears. A DNA-origami based experiment with short spacer strands could, thus, incorrectly produce icosahedra instead of snub-cube.

It is instructive to examine the yield at a density typical of the DNA-origami case, $\rho \approx 10^{-5}$. A small value of density disfavors the aggregation process and, as such, this negative contribution needs to be compensated by a smaller temperature. Fig. 7(b) shows that results similar to the $T = 0.10$ are, indeed, found for larger $\cos\theta$. However, in the most directional case, now only monomers are expected.

It is also instructive to look at the yield of the different clusters as a function of density and temperature. Figure 8(a) shows the yield of the snub-cube as a function of sample density for the wide patch angle $\cos\theta = 0.93$. The data for $T = 0.08$ and $T = 0.09$ are calculated under the verified assumption that at $T = 0.10$, in the CGCMC simulations, the bottom of the energy landscape is properly sampled for all N. These data suggest that at $T = 0.08$ and below, the snub-cube should form with yield one (similar results hold for $\cos\theta = 0.96$). The same $Y(N)$ data are shown as a function of T for different cluster size N and different densities in Fig. 8(b).

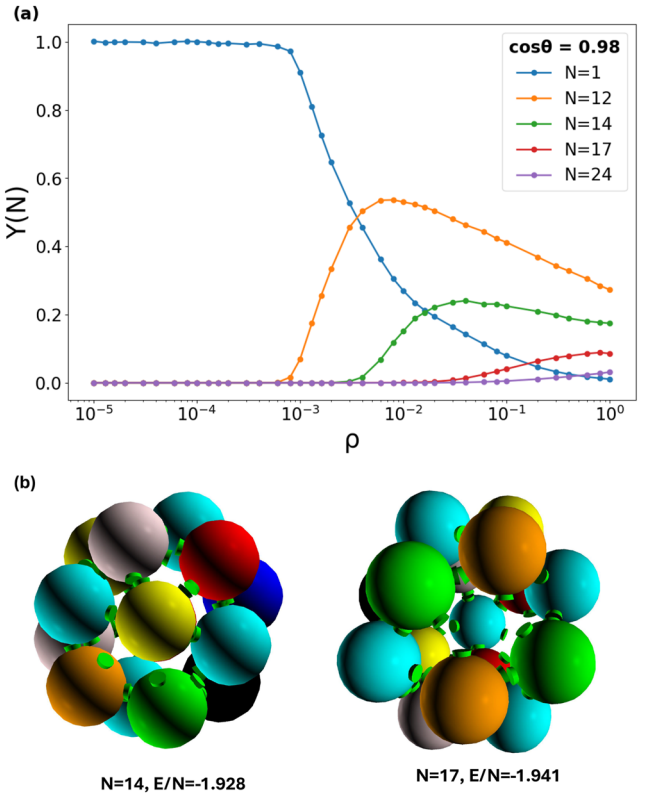

FIG. 9. (a) Yield of different clusters for $\cos\theta = 0.98$ and $T = 0.10$. Note that $\rho = 1$ is equivalent to a packing fraction of ≈0.5. (b) Lowest energy clusters with $N = 14$ (left) and $N = 17$ (right) for the case $\cos\theta = 0.98$. Here, different colors indicate different particle species.

For the most directional case ($\cos\theta = 0.98$), at $T = 0.10$ [see Fig. 9(a)], the targeted self-assembly process fails and monomers are found to coexist with several clusters, including $N = 12$, $N = 14$, and $N = 17$ clusters. At this T, no evidence for $N = 24$ is found for any reasonable density. The lowest energy $N = 14$ cluster, despite the fact that its energy per particle is only −1.928 (27 formed bonds out of 35), is a gyroelongated hexagonal bipyramid with 24 triangular faces, 14 vertices, and 36 edges, a close shell formed by two rotated hexagonal rings capped by a particle at the top and bottom. The lowest energy $N = 17$ cluster, with an energy of −1.941 (33 bonds out of 42), is instead an incomplete cage. Both clusters are shown in Fig. 9(b).

In brief, for $\cos\theta = 0.93$ and $\cos\theta = 0.96$, the snub-cube maximum yield is reached in the vicinity of T = 0.10 up to a total density equal to $\rho = 10^{-5}$. In the case of $\cos\theta = 0.98$, the snub-cube does not form.

IV. CONCLUSIONS

In this work, we have investigated the self-assembly of a finite target structure, the snub cube, using a combination of SAT-based interaction design[23] and cluster free-energy calculations. Our results highlight a central lesson: designing interactions that stabilize a target as the ground state is not sufficient to ensure its formation at finite temperature. Even when competing structures are energetically penalized, they can still emerge as thermodynamically relevant states once entropic contributions are taken into account.

In particular, we have shown that the balance between bond directionality and geometric compatibility plays a crucial role in determining the assembly outcome. While more directional interactions improve energetic selectivity, they also reduce the configurational entropy of the target structure and increase the sensitivity to geometric mismatch. Ill-fitting subunits, namely subunits whose patch geometry does not precisely match that required by the target structure, may stabilize off-target structures. As a result, competing aggregates, such as the icosahedron in the present case, can become stabilized by entropy, despite having fewer satisfied bonds. This leads to a rich free-energy landscape in which multiple cluster sizes can coexist or even dominate under experimentally relevant conditions.

These findings point to a fundamental limitation of design strategies based solely on ground-state optimization: the thermodynamic stability of the target structure must be assessed at finite temperature, where entropy can qualitatively alter the assembly behavior. In this sense, interaction design should be viewed as a joint optimization of energy and entropy, rather than of energy alone.

The CGCMC approach provides a powerful framework to address this problem, enabling a direct and quantitative determination of the free-energy landscape of self-assembling systems without relying on simplifying assumptions. This allows one to predict not only the target structure but also the competing pathways and the conditions under which they become relevant. In the present case, this analysis provides concrete guidance on how parameters, such as bond flexibility and temperature, can be tuned to optimize the yield of the desired cluster.

More broadly, our work suggests that combining inverse design strategies, such as SAT-assembly, with explicit free-energy

calculations offers a promising route toward the rational design of complex self-assembling systems that remain robust under realistic conditions.

ACKNOWLEDGMENTS

We dedicate this work to Christoph Dellago in celebration of his 60th birthday. We thank Diogo Pinto for his valuable help in the early stages of the project. We acknowledge computational support from Cineca ISCRAB initiative and ICSC-Centro Nazionale di Ricerca in High Performance Computing, Big Data and Quantum Computing, funded by the European Union "NextGenerationEU." This result is part of a project that has received funding from the European Research Council (ERC) under the European Union's Horizon 2020 research and innovation program (Grant Agreement No. 101040035) (to P.Š.).

AUTHOR DECLARATIONS

Conflict of Interest

The authors have no conflicts to disclose.

Author Contributions

Luigi Graziano: Data curation (equal); Formal analysis (equal); Writing – original draft (equal). **Niccolò Tedeschi**: Formal analysis (equal). **Petr Šulc**: Conceptualization (equal); Writing – original draft (equal). **John Russo**: Conceptualization (lead); Data curation (lead); Formal analysis (equal); Writing – original draft (lead). **Francesco Sciortino**: Conceptualization (equal); Data curation (equal); Formal analysis (equal); Writing – original draft (equal).

DATA AVAILABILITY

The data that support the findings of this study are available within the article.

APPENDIX A: CLUSTER MONTE CARLO DETAILS

In the CGCMC method, the window of explored cluster sizes N is separated in several distinct overlapping windows. A window is, thus, identified by a lower $N_{\min}$ and a maximum $N_{\max}$ number of particles. Insertion moves increasing N beyond $N_{\max}$ are rejected. Similarly, deletion moves reducing N below $N_{\min}$ are also rejected. In addition to single particle insertion and deletion moves, roto-translational moves are implemented. In this type of moves, the center of the particle is translated by a random number between $\pm 0.075\sigma$ and simultaneously rotated around a randomly chosen axis by a random angle between ± 0.0075 rad. In the insertion move (one every 100 roto-translational moves), a particle of a random species is added, in a random orientation, to the system in a position $\mathbf{r}$ in a shell at distance $\sigma < |\mathbf{r}| < \sigma + \Delta$, where Δ is the interaction range of the Kern–Frenkel potential [see Eq. (1)] and σ is the hard core diameter. The spherical shell has volume $V_{ins} = \frac{4}{3}\pi((\sigma+\Delta)^3 - \sigma^3)$. Indicating with ΔE the change in energy, the acceptance probability for the insertion move of a particle of type k is (indicating with z_k the activity of particle k),

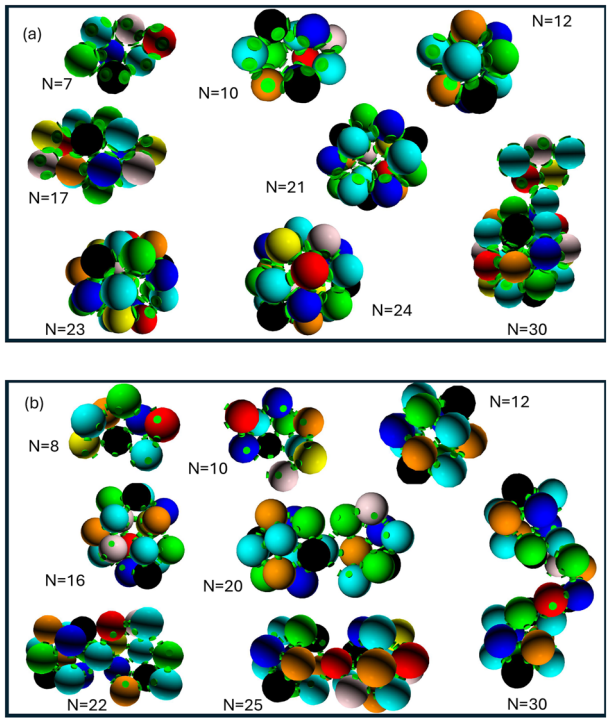

FIG. 10. Typical clusters sampled during the CGCMC for $\cos\theta = 0.93$ (a) and $\cos\theta = 0.98$ (b) at T = 0.10. Different colors indicate different particle types.

$$acc(N_k \to N_{k+1}) = \frac{(N-1)z_k V_{ins} e^{-\beta\Delta E}}{\sigma^3 N_k n_{neigh}}. \tag{A1}$$

Note that if the randomly selected point $\mathbf{r}$ is part of the shell of n_{neigh} distinct particles (by definition $n_{neigh} \geq 1$), this point will be sampled n_{neigh} times. To correct for this, the acceptance probability is divided by n_{neigh}.

In the deletion move (one every 100 roto-translational moves), a particle type is first selected randomly and then one of the existing particle of that type (if it exists) is randomly deleted. The deletion probability for a particle of type k is

$$acc(N_k \to N_{k-1}) = \sigma^3 \frac{e^{\beta\Delta E} N_k}{(N-1)z_k V_{ins}}. \tag{A2}$$

Moves that break the cluster into pieces or moves that generate more than one cluster in the system are rejected. The algorithm implemented follows the original scheme proposed in Ref. 52 and previously applied to dipolar spheres[54] and patchy colloids.[53] Figure 10 shows typical clusters sampled in the CGCMC simulations.

APPENDIX B: INTERACTION DESIGN AND SAT CONSTRAINTS

The interaction rules defining the building blocks are specified in terms of particle species and complementary patch–patch interactions.

Each particle carries five patches, whose positions are fixed by the underlying icosahedral scaffold. The assignment of interaction "colors" to the patches of each species is reported in Table II. Each color represents a specific binding type.

Complementary interactions are defined through a one-to-one matching between colors. Only the pairs listed in Table III are attractive; all other interactions are non-binding.

The interaction scheme was obtained using the SAT-assembly framework by imposing the following constraints:

1. **One-to-one color complementarity.** Each interaction color is assigned a unique complementary partner, and no color can interact with more than one counterpart. This enforces a strictly one-to-one binding scheme, ensuring that each patch type participates in a single, well-defined interaction.
2. **No self-complementary interactions.** Colors are not allowed to bind to themselves. This constraint is motivated by experimental considerations, as self-complementary DNA sequences (palindromic sequences) are more difficult to design and to reliably incorporate into DNA-origami scaffolds.
3. **Suppression of face-to-face aggregation of icosahedra.** Two icosahedral clusters are only allowed to interact through a single bond. Configurations in which two icosahedra bind by sharing an entire face (thereby satisfying all three bonds associated with that face) are explicitly forbidden.
4. **Exclusion of fully bonded icosahedral structures.** The interaction matrix is constructed so that a fully bonded icosahedron cannot be realized. This prevents the icosahedral geometry from becoming a competing ground-state structure.

These constraints ensure that the target snub-cube structure is uniquely favored at the level of the interaction network, while suppressing competing assemblies at the energetic level.

TABLE II. Patch-color assignment for the eight particle species. Each row lists the five interaction colors associated with the patches of a given species.

Species	Patch colors				
1	13	16	3	13	2
2	22	11	10	19	13
3	15	13	9	6	7
4	13	8	20	13	2
5	13	4	17	13	2
6	18	14	10	19	13
7	6	12	6	1	6
8	5	13	21	6	7

TABLE III. Complementary color pairs defining the interaction matrix. Each color interacts exclusively with its paired counterpart.

Color	Complementary color
1	7
2	19
3	4
5	15
6	13
8	17
9	14
10	12
11	21
16	20
18	22

APPENDIX C: EQUILIBRIUM BETWEEN MONOMERS AND SNUB-CUBE

The low T data for $\cos\theta = 0.93$ and $\cos\theta = 0.96$ (for example Fig. 7) show that the sample is composed by monomers or snub-cubes in a relative concentration dictated by the sample density. All other clusters are irrelevant. Under this condition, it is possible to calculate the theoretical expression for $Y[24]$, knowing that the energy per particle of the snub-cube is 2.5 ϵ, while it is zero for the monomer. From standard thermodynamics (assuming $\lambda^3 = 1$), one has (indicating for simplicity with Z_{24} and Z_1 the partition function of the snub-cube and of a monomer)

$$N_{24} = Z_{24}\prod_{s=1}^{8}\left(\frac{N_{1,s}}{Z_1}\right)^{n_s}, \tag{C1}$$

[with $n_s = (2,3,3,2,2,3,6,3)$], and

$$\frac{Z_{24}}{Z_1} = e^{24\beta(2.5\epsilon+Ts)}, \tag{C2}$$

where s is the entropy per particle in the snub-cube configuration, which can be considered as a fit parameter or extracted from the numerical results in Fig. 4. In terms of number densities (dividing by V),

$$\rho_{24} = \frac{Z_{24}}{Z_1}\prod_{s=1}^{8}\rho_{1,s}^{n_s} = \frac{Z_{24}}{Z_1}\rho_1^{24}\prod_{s=1}^{8}\left(\frac{n_s}{24}\right)^{n_s}, \tag{C3}$$

which need to be solved with the constraint ($\rho_1 = \sum_s \rho_{1,s}$),

$$\rho = 24\rho_{24} + \rho_1, \tag{C4}$$

to obtain the full $Y[24]$ vs ρ function. Note that the product $\prod_{s=1}^{8}\left(\frac{n_s}{24}\right)^{n_s} = 1.1898\ 10^{-21}$ accounts for the mixing entropy of the monomeric state. Indeed, it can be expressed in the more familiar form, defining the concentration $x_s \equiv n_s/24$ of the species s in the snub-cube,

$$\prod_{s=1}^{8}\left(\frac{n_s}{24}\right)^{n_s} = e^{24\sum_s x_s \ln x_s} = e^{-2.007\ 52\times 24} \equiv e^{24 s_{\mathrm{mix}}/k_B}. \tag{C5}$$

Since $Y[24] = 0.5$ corresponds to $\rho_1 = \frac{\rho}{2}$ and $\rho_{24} = \frac{\rho}{48}$, the expression

$$\frac{\rho}{48} = e^{24\beta(2.5\epsilon+T(s+s_{\mathrm{mix}}))}\left(\frac{\rho}{2}\right)^{24} \tag{C6}$$

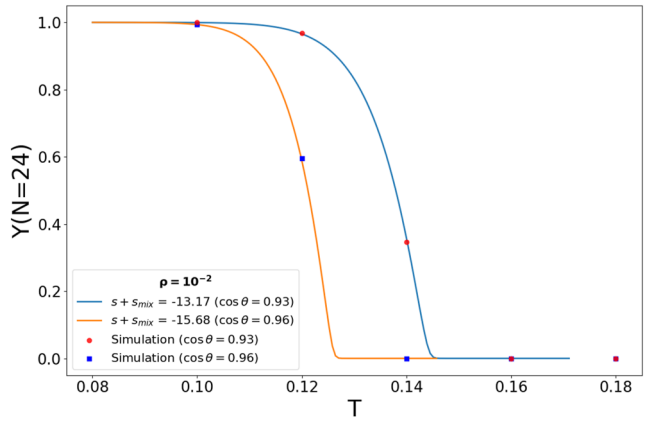

FIG. 11. Theory based on only two clusters (monomers and snub-cube) and MC results for $Y[24]$ vs T. Here, $s + s_{mix}$ (in units of k_B) is 13.17 and 15.68, respectively, for $\cos\theta = 0.93$ and $\cos\theta = 0.96$.

provides the locus in the $T - \rho$ plane where half of the particles are part of N = 24 clusters and half of them are in monomeric state. With some simple algebra, Eq. (C6) gives

$$\rho = e^{-\frac{24}{23}(2.5\epsilon/k_BT+(s+s_{\rm mix})/k_B)-\frac{1}{23}\ln 48}. \tag{C7}$$

Since in the ground state, s does not depend on T, this expression provides the "melting" curve $T(\rho)$ of the snub-cube.

APPENDIX D: YIELD OF N = 24 VS TEMPERATURE AT FIXED DENSITY

With the same approximation as the previous subsection, it is possible to calculate theoretically the yield of the snub-cube. The expression requires only the entropy per particle of the snub-cube, a quantity that is provided by the CGCMC [see Fig. 4(c)]. From Eq. (C3), we have

$$\rho_{24} = e^{24(2.5\beta\epsilon+(s+s_{\rm mix})/k_B)}(\rho - 24\rho_{24})^{24}, \tag{D1}$$

and taking the log,

$$2.5\beta\epsilon + \frac{(s+s_{\rm mix})}{k_B} + \ln(\rho - 24\rho_{24}) - \frac{\ln(\rho_{24})}{24} = 0. \tag{D2}$$

Going from density to yield by substituting $Y[24] = \frac{24\rho_{24}}{\rho}$, one obtains the final result,

$$\frac{\ln(Y[24])}{24} - \ln(1 - Y[24]) = 2.5\beta\epsilon + \frac{s+s_{\rm mix}}{k_B} + \frac{\ln(24)}{24} + \frac{23}{24}\ln\rho. \tag{D3}$$

Figure 11 compared the yield theoretically calculated according to Eq. (D3) with the CGCMC results.

REFERENCES

[1]G. M. Whitesides and B. Grzybowski, "Self-assembly at all scales," Science **295**, 2418–2421 (2002).
[2]S. Whitelam and R. L. Jack, "The statistical mechanics of dynamic pathways to self-assembly," Annu. Rev. Phys. Chem. **66**, 143–163 (2015).
[3]G. van Anders, N. K. Ahmed, R. Smith, M. Engel, and S. C. Glotzer, "Entropically patchy particles: Engineering valence through shape entropy," ACS Nano **8**, 931–940 (2013).
[4]S. Sacanna, M. Korpics, K. Rodriguez, L. Colón-Meléndez, S.-H. Kim, D. J. Pine, and G.-R. Yi, "Shaping colloids for self-assembly," Nat. Commun. **4**, 1688 (2013).
[5]J. Metson, S. Osat, and R. Golestanian, "Continuous-time multifarious systems. I. Equilibrium multifarious self-assembly," J. Chem. Phys. **163**, 124904 (2025).
[6]M. Holmes-Cerfon and M. Wyart, "Hierarchical self-assembly for high-yield addressable complexity at fixed conditions," Proc. Natl. Acad. Sci. U. S. A. **122**, e2500245122 (2025).
[7]B. Hsiao-Yen Wei, C. Levi Petix, Q. Chen, M. P. Howard, and J. Mittal "Design of simple interactions to assemble complex crystals from binary mixtures of colloidal particles," Mol. Syst. Des. Eng. **11**(4), 324–335 (2026).
[8]X. Xia, Y. Peng, K. Ki Li, and R. Ni, "Designed self-assembly of programmable colloidal atom-electron equivalents," Rep. Prog. Phys. **88**, 078101 (2025).
[9]M. F. Hagan and G. M. Grason, "Equilibrium mechanisms of self-limiting assembly," Rev. Mod. Phys. **93**, 025008 (2021).
[10]L. Koehler, M. Eder, V. Ouazan-Reboul, C. Karfusehr, A. Zelenskiy, P. Ronceray, F. C. Simmel, and M. Lenz, "Topological defect engineering enables size and shape control in self-assembly," arXiv:2504.13073 (2025).
[11]S. Liu, T. E. Videbæk, and W. B. Rogers, "Taming polymorphism of tubule self-assembly using templated growth," J. Chem. Phys. **164**, 064903 (2026).
[12]G. N. Jones, P. W. A. Schoenhoefer, and S. C. Glotzer, "Using particle shape to control defects in colloidal crystals on spherical interfaces," Soft Matter **22**, 2558 (2026).
[13]Zhang, A. S. Keys, T. Chen, and S. C. Glotzer, "Self-assembly of patchy particles into diamond structures through molecular mimicry," Langmuir **21**, 11547–11551 (2005).
[14]C. Karner, C. Dellago, and E. Bianchi, "Design of patchy rhombi: From close-packed tilings to open lattices," Nano Lett. **19**, 7806–7815 (2019).
[15]C. Karner, C. Dellago, and E. Bianchi, "Hierarchical self-assembly of patchy colloidal platelets," Soft Matter **16**, 2774–2785 (2020).
[16]H. Liu, M. Matthies, J. Russo, L. Rovigatti, R. P. Narayanan, T. Diep, D. McKeen, O. Gang, N. Stephanopoulos, F. Sciortino *et al.*, "Inverse design of a pyrochlore lattice of DNA origami through model-driven experiments," Science **384**, 776–781 (2024).
[17]A. Neophytou, F. Sciortino, and J. Russo, "Designing the self-assembly of disordered materials via color frustration," Adv. Mater. **37**, 2502136 (2025).
[18]S. Torquato, "Inverse optimization techniques for targeted self-assembly," Soft Matter **5**, 1157–1173 (2009).
[19]W. D. Piñeros, B. A. Lindquist, R. B. Jadrich, and T. M. Truskett, "Inverse design of multicomponent assemblies," J. Chem. Phys. **148**, 104509 (2018).
[20]Y. Ma and A. L. Ferguson, "Inverse design of self-assembling colloidal crystals with omnidirectional photonic bandgaps," Soft Matter **15**, 8808–8826 (2019).
[21]E. G. Noya and J. P. K. Doye, "A one-component patchy-particle icosahedral quasicrystal," ACS Nano **19**, 13714–13722 (2025).
[22]G. van Anders, D. Klotsa, A. S. Karas, P. M. Dodd, and S. C. Glotzer, "Digital alchemy for materials design: Colloids and beyond," ACS Nano **9**, 9542–9553 (2015).
[23]J. Russo, F. Romano, L. Kroc, F. Sciortino, L. Rovigatti, and P. Šulc, "Sat-assembly: A new approach for designing self-assembling systems," J. Phys.: Condens. Matter **34**, 354002 (2022).
[24]S. Chatterjee and W. M. Jacobs, "Multiobjective optimization for targeted self-assembly among competing polymorphs," Phys. Rev. X **15**, 011075 (2025).
[25]L. Cademartiri and K. J. M. Bishop, "Programmable self-assembly," Nat. Mater. **14**, 2–9 (2015).
[26]A. V. Tkachenko, "Structural and compositional complexities of hierarchical self-assembly: A hypergraph approach," J. Chem. Phys. **164**, 044113 (2026).
[27]A. W. Long and A. L. Ferguson, "Rational design of patchy colloids via landscape engineering," Mol. Syst. Des. Eng. **3**, 49–65 (2018).
[28]J. O'Leary, R. Mao, E. J. Pretti, J. A. Paulson, J. Mittal, and A. Mesbah, "Deep learning for characterizing the self-assembly of three-dimensional colloidal systems," Soft Matter **17**, 989–999 (2021).

[29]G. M. Coli, E. Boattini, L. Filion, and M. Dijkstra, "Inverse design of soft materials via a deep learning–based evolutionary strategy," Sci. Adv. **8**, eabj6731 (2022).
[30]M. Dijkstra and E. Luijten, "From predictive modelling to machine learning and reverse engineering of colloidal self-assembly," Nat. Mater. **20**, 762–773 (2021).
[31]A. Lizano-Villalobos, F. Ma, W. Tang, W. Sun, and X. Tang, "Machine learning-based optimal control for colloidal self-assembly," AIChE J. **72**(7), e70389 (2026).
[32]W. Liu, M. Tagawa, H. L. Xin, T. Wang, H. Emamy, H. Li, K. G. Yager, F. W. Starr, A. V. Tkachenko, and O. Gang, "Diamond family of nanoparticle superlattices," Science **351**, 582–586 (2016).
[33]N. C. Seeman, *Structural DNA Nanotechnology* (Cambridge University Press, 2015).
[34]P. G. Moerman, C.-H. Chou, T. E. Videbæk, W. B. Rogers, and R. Schulman, "A DNA-encoded recipe to direct multistage colloidal assembly," Proc. Natl. Acad. Sci. U. S. A. **123**, e2527410123 (2026).
[35]P. W. K. Rothemund, "Folding DNA to create nanoscale shapes and patterns," Nature **440**, 297–302 (2006).
[36]C. Karfusehr, M. Eder, H. Y. Yang, B. Beinsteiner, M. Jasnin, and F. C. Simmel, "Self-assembled cell-scale containers made from DNA origami membranes," Nat. Mater. **25**, 502–510 (2025).
[37]S. M. Douglas, H. Dietz, T. Liedl, B. Högberg, F. Graf, and W. M. Shih, "Self-assembly of DNA into nanoscale three-dimensional shapes," Nature **459**, 414–418 (2009).
[38]E. S. Andersen, M. Dong, M. M. Nielsen, K. Jahn, R. Subramani, W. Mamdouh, M. M. Golas, B. Sander, H. Stark, C. L. P. Oliveira *et al.*, "Self-assembly of a nanoscale DNA box with a controllable lid," Nature **459**, 73–76 (2009).
[39]G. Posnjak, X. Yin, P. Butler, O. Bienek, M. Dass, S. Lee, I. D. Sharp, and T. Liedl, "Diamond-lattice photonic crystals assembled from DNA origami," Science **384**, 781–785 (2024).
[40]K. Binder and W. Kob, *Glassy Materials and Disordered Solids: An Introduction to Their Statistical Mechanics* (World Scientific, 2011).
[41]E. Zaccarelli, "Colloidal gels: Equilibrium and non-equilibrium routes," J. Phys.: Condens. Matter **19**, 323101 (2007).
[42]S. Jungblut and C. Dellagoa, "Pathways to self-organization: Crystallization via nucleation and growth," Eur. Phys. J. E **39**, 77 (2016).
[43]N. A. Mahynski, R. Mao, E. Pretti, V. K. Shen, and J. Mittal, "Grand canonical inverse design of multicomponent colloidal crystals," Soft Matter **16**, 3187–3194 (2020).
[44]J. Peña, L. Dagdug, and D. Reguera, "Kinetic description of viral capsid self-assembly using mesoscopic non-equilibrium thermodynamics," Entropy **27**, 281 (2025).
[45]N. W. Hackney and G. Grason, "Geometrically frustrated assembly at finite temperature: Phase transitions from self-limiting to bulk states," Phys. Rev. E **112**, 065419 (2025).
[46]A. Gnidovec and S. Čopar, "Controlling curvature of self-assembling surfaces via patchy particle design," Commun. Phys. **8**, 467 (2025).
[47]D. E. P. Pinto, P. Šulc, F. Sciortino, and J. Russo, "Design strategies for the self-assembly of polyhedral shells," Proc. Natl. Acad. Sci. U. S. A. **120**, e2219458120 (2023).
[48]T. L. Hill, *An Introduction to Statistical Thermodynamics* (Courier Corporation, 2012).
[49]F. Romano, J. Russo, L. Kroc, and P. Šulc, "Designing patchy interactions to self-assemble arbitrary structures," Phys. Rev. Lett. **125**, 118003 (2020).
[50]W. Bol, "Monte Carlo simulations of fluid systems of waterlike molecules," Mol. Phys. **45**, 605–616 (1982).
[51]N. Kern and D. Frenkel, "Fluid–fluid coexistence in colloidal systems with short-ranged strongly directional attraction," J. Chem. Phys. **118**, 9882–9889 (2003).
[52]D. J. Kraft, R. Ni, F. Smallenburg, M. Hermes, K. Yoon, D. A. Weitz, A. van Blaaderen, J. Groenewold, M. Dijkstra, and W. K. Kegel, "Surface roughness directed self-assembly of patchy particles into colloidal micelles," Proc. Natl. Acad. Sci. U. S. A. **109**, 10787–10792 (2012).
[53]T. Vissers, F. Smallenburg, G. Munaò, Z. Preisler, and F. Sciortino, "Cooperative polymerization of one-patch colloids," J. Chem. Phys. **140**, 144902 (2014).
[54]M. Ronti, L. Rovigatti, J. M. Tavares, A. O. Ivanov, S. S. Kantorovich, and F. Sciortino, "Free energy calculations for rings and chains formed by dipolar hard spheres," Soft Matter **13**, 7870–7878 (2017).
[55]P. Virnau and M. Müller, "Calculation of free energy through successive umbrella sampling," J. Chem. Phys. **120**, 10925–10930 (2004).
[56]F. Sciortino, "Basic concepts in self-assembly," in *Soft Matter Self-Assembly* (IOS Press, 2016), pp. 1–17.